PAPER

Optical and structural properties of AlN thin films deposited on different faces of sapphire substrates

To cite this article: Junhua Yin *et al* 2021 *Semicond. Sci. Technol.* **36** 045012

View the article online for updates and enhancements.

You may also like

- AlN films deposited by dc magnetron sputtering and high power impulse magnetron sputtering for SAW applications
K Ait Aissa, A Achour, O Elmazria et al.
- Preparation of single crystalline AlN thin films on ZnO nanostructures by atomic layer deposition at low temperature
Yuan Zhang, Jia-Jia Tao, Hong-Yan Chen et al.
- Effect of growth temperature of an AlN intermediate layer on the growth mode of AlN grown by MOCVD
W Tian, W Y Yan, J N Dai et al.

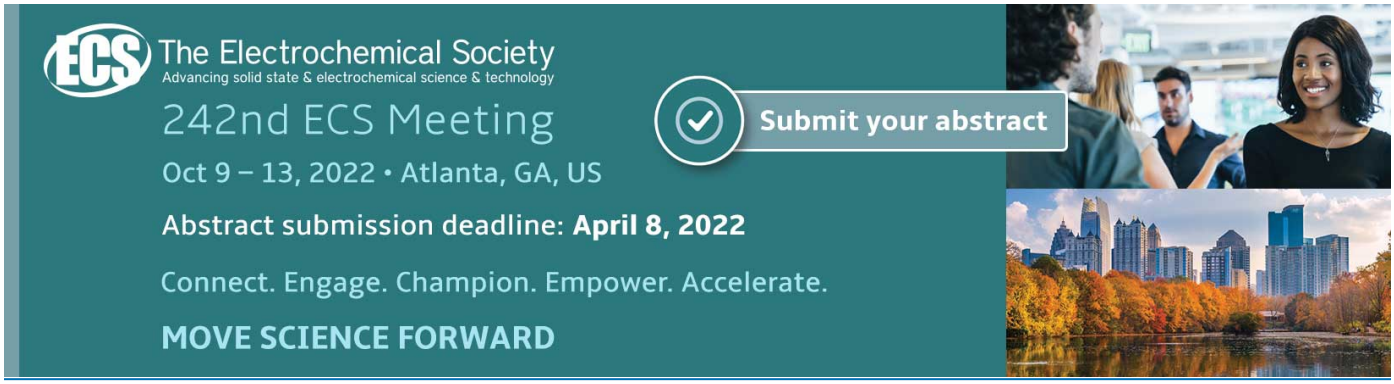

This content was downloaded from IP address 159.226.165.244 on 01/03/2022 at 03:06

IOP Publishing Semiconductor Science and Technology
Semicond. Sci. Technol. **36** (2021) 045012 (13pp) https://doi.org/10.1088/1361-6641/abe3c5

Optical and structural properties of AlN thin films deposited on different faces of sapphire substrates

Junhua Yin[1], Bangdi Zhou[1], Liang Li[2], Yao Liu[1], Wei Guo[2], Devki N Talwar[3], Kaiyan He[1], Ian T Ferguson[4], Lingyu Wan[1,5] and Zhe Chuan Feng[1,5,6]

[1] Laboratory of Optoelectronic Materials and Detection Technology, Center on Nano-Energy Research, Guangxi Key Laboratory for the Relativistic Astrophysics, School of Physical Science and Technology, Guangxi University, Nanning 530004, People's Republic of China
[2] Ningbo Institute of Materials Technology and Engineering, Chinese Academy of Sciences Ningbo, Zhejiang 315201, People's Republic of China
[3] Department of Physics, University of North Florida, Jacksonville, FL 32224, United States of America
[4] Southern Polytechnic College of Engineering and Engineering Technology, Kennesaw University, Kennesaw, GA 30144, United States of America
[5] State Key Laboratory of Luminescence and Applications, Changchun Institute of Optics, Fine Mechanics and Physics, Chinese Academy of Sciences, Changchun 130033, People's Republic of China
[6] Science Exploring Lab, Arbour Glenn Drive, Lawrenceville, GA 30043, United States of America

E-mail: zcfeng@ntu.edu.tw, fengzhechuan@gmail.com and gredhky@gxu.edu.cn

Received 26 October 2020, revised 22 January 2021
Accepted for publication 5 February 2021
Published 4 March 2021

Abstract

We report the comprehensive spectroscopic results of AlN thin films deposited on the *A*-, *R*- and *C*-surfaces of sapphire substrates by radio frequency magnetron sputtering. The optical and structural properties of the epitaxial-grown AlN films were characterized using various techniques of high-resolution x-ray diffraction spectroscopy, x-ray photoelectron spectroscopy, Raman scattering spectroscopy, spectroscopic ellipsometry and associated analytical tools. Our large number of measurement results clearly show that sapphire substrates of different polarities have effects on the surface roughness, dislocation density, grain size, microstrain, and surface oxygen binding capacity of the film grown on its surface. The results obtained from Ellipsometry measurements show that the thickness, band gap and roughness of AlN films grown on *C*-plane sapphire are the smallest among the three samples. After careful analyses of the variable temperature Raman spectra, as the temperature rises from 80 K to 800 K, the AlN film has always exhibited tensile stress. In the same temperature range, the tensile stress of the AlN film grown on the *C*-plane sapphire has the greatest effect with temperature. The lifetime of E_2 (high) phonons gradually decays with the increase of temperature.

Keywords: aluminum nitride, sapphire, magnetron sputtering, x-ray photoelectron spectroscopy (XPS), temperature-dependent Raman

(Some figures may appear in color only in the online journal)

1. Introduction

Aluminum nitride is a very important semiconductor material [1–5]. Compared with other III-nitrides, it has the widest direct band gap of 6.2 eV at room temperature, high stability, high volume resistivity (10^{11}–10^{13}), high thermal conductivity (285 W mK^{-1}), high breakdown field (1.2–1.8 $\times$ 10^6 V cm^{-1}) [6–13]. These characteristics make AlN have a wide range of applications, in optoelectronic and acoustoelectronic devices, such as surface wave and bulk acoustic wave devices [14–16], field emission displays [17], light-emitting diodes [18] and laser diodes [19–24]. AlN is widely used as a buffer layer for

 © 2021 IOP Publishing Ltd Printed in the UK

epitaxial growth of gallium nitride/aluminum gallium nitride [25, 26]. It also has broad application prospects in the fields of biomedicine, solid-state light sources, and air (water) sterilization [27–31]. Up to now, III-nitride structures have been grown on heterogeneous substrates of sapphire, silicon, SiC, etc [32], and those structures mainly prepared by three deposition methods of metal organic chemical vapor deposition, molecular beam epitaxy and hydride vapor phase epitaxy [33, 34]. In recent years, researchers have reported that magnetron sputtering can be used to grow single crystal AlN films [35]. Magnetron sputtering is a type of physical vapor deposition. In contrast, magnetron sputtering equipment, which has a low cost and is easy to control, is widely used in the film deposition of metals, semiconductors, insulators, and various compounds [36, 37].

At the same time, the films grown by magnetron sputtering have some shortcomings. The bombardment of high-energy particles in the magnetron sputtering process will cause various defects in the film. To prepare high-quality AlN films, the setting of process parameters is very important [38]. Due to the influence of thermal mismatch and lattice mismatch, the growth of AlN films on the C surface is also extremely chaotic [39, 40]. In addition, the higher growth temperature of the substrate is conducive to the migration of Al atoms. The atmosphere environment in the magnetron sputtering process also has a great influence on the growth of AlN films. Because of the strong affinity between Al atoms and O atoms, oxygen contamination is easily formed in AlN films [41, 42]. Finally, during the growth process, the total air pressure also has a great influence on the growth of the film. If the total air pressure is not well controlled, it is easy to form N vacancies and reduce the quality of the film [43].

In this work, magnetron sputtering technology was employed to grow a series of AlN films on *A, R* and *C* sapphire. We used high-resolution x-ray diffraction (HR-XRD), spectroscopic ellipsometry (SE), optical transmission (OT), x-ray photoelectron spectroscopy (XPS) and Raman scattering (RS) to comprehensively analyze some of the valuable properties of these AlN epitaxial films. We analyzed the structural characteristics and orientation of the film through HR-XRD technology, and understand the difference in micro-strain, grain size and dislocation density. OT and SE spectra were used to obtain the band gap value *Eg* of AlN films grown on sapphire substrates on different sides, followed by the differences in their optical constants and transmittance. We used XPS to analyze the valence state of the film and the thickness of its surface oxide. Through variable temperature RS spectroscopy, the relationship between the spectral line width, stress, Raman shift and phonon lifetime of E_2 (high) AlN films with different polarities with temperature can be obtained. To study and analyze, quantitatively and in phenomenology, the influence of sapphire substrates with different crystal planes on the crystal structure and optical properties of AlN films, this can provide useful reference information for further penetrative studies and the manufacture of high-quality AlN devices.

2. Experiments

Radio frequency magnetron sputtering technology was employed to prepare AlN thin films. Three AlN films grown on the *A-, R-* and *C*-plane sapphire are referred to as ANa, ANr and ANc, respectively. Al was used as the target material. The gas environment is a mixed gas of N_2 and Ar. When the Al target material is sputtered, the sputtered high-energy Al particles will interact with the N in N_2. The atoms form AlN, which is deposited on the substrate material. The equipment used is a customized JGP450 high-vacuum sputtering system with an ultimate vacuum of 6×10^{-6} Pa, and is equipped with AE MDX 1k and AE Pinnacle Plus + 5/5 intermediate frequency pulse DC power supplies and Comdel CV −1000 RF power supply, used to provide different sputtering conditions. High-temperature thermal annealing of magnetron sputtered AlN film can reduce the content of threading dislocations and other point defects in the film, thereby improving the crystal quality of the AlN film. The high-temperature equipment we use is a model of Hangzhou Aotem Optoelectronics Co., Ltd UTI-PVT-D075H PVT single crystal vapor deposition furnace. Since physical vapor transport (PVT) growth itself requires a particularly high temperature, its high temperature cavity can be used for ultra-high temperature thermal annealing. It adopts double tungsten resistance heating method, the maximum power of the heater located below can reach 51 kW, and the maximum working temperature is as high as 2400 °C. It can provide high-purity N_2, high-purity H_2, argon, ammonia, etc as the working atmosphere. Both sets of heaters adopt advanced computer control technology for independent control, which can realize flexible and precise adjustment of the temperature field in the furnace. The films were characterized by a variety of spectroscopic techniques, including HR-XRD, XPS, RS spectroscopy, OT and SE, etc.

First, the crystal orientation and structure of the sample were characterized by HR-XRD (SMARTLAB3KW), using CuK_α ($\lambda = 0.15406$ nm) radiation. The XRD 2θ scans were performed in the range of 25–140°, with a step size of 0.1°. Secondly, a variable angle spectroscopic ellipsometer (VASE; ME-L ellipsometer, Wuhan Eoptics Technology Co. Ltd China) was used to analyze the thickness, roughness, optical constant and band gap of the film. We then used an ultraviolet–visible photometer (Zolix OmniAs, China) with a deuterium lamp to study and analyze the absorption characteristics of the AlN films. The surface element composition of the sample was characterized by XPS (ESCALAB 250XI), and 284.8 eV of C1s was used to calibrate the full spectrum and narrow spectrum of all XPS, and the XPSpesk4.1 program was used to fit the narrow spectrum. Finally, by using a miniature Raman spectrometer, Raman measurements were performed on three samples under the excitation of 266 nm (FQCW266) and 325 nm (IK3301R-G). All the above measurements were performed at room temperature. Temperature-dependent RS (80–800 K) measurements was performed using Linkam heating system (THMS600) and water circulator under an excitation laser wavelength of 266 nm, followed with penetrative analyses.

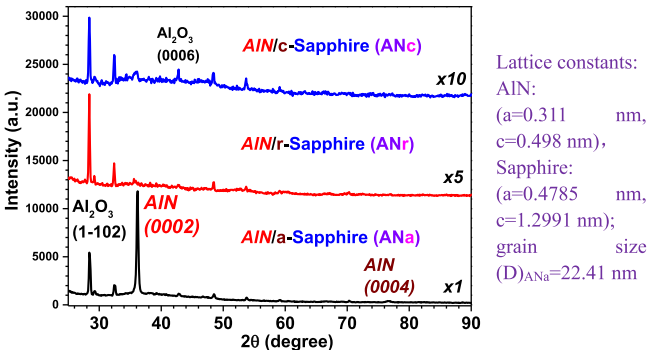

Figure 1. XRD patterns of three AlN films, with multiplying 1, 5 and 10 times for ANa, ANr and ANc, respectively.

3. Results and discussion

3.1. Structural properties of the grown AlN films: lattice orientations and grain sizes

In order to study the structural characteristics of three AlN films and compare their crystal quality intuitively, XRD tests were performed on three samples, and the crystal quality of the crystals was compared by the half-height width of the XRD pattern. The results are shown in figure 1. ANa shows a strong diffraction peak of AlN (0002) crystal plane, with the 2θ value of around 36°, while for ANr and ANc spectra by magnifying 5 times and 10 times, respectively, we can observe the faint diffraction peaks of AlN (0002) crystal plane. This phenomenon may be caused by lattice matching, which is relative to the sapphire substrate, ANr and ANc have more dislocations, which means that the crystal qualities of these two films are poorer than ANa. Weak signals around 32° and 48° in the XRD spectra of figure 1 may be noise signals during the tests. In addition, ANa can also detect the (0004) plane second-order diffraction peak. Which was appeared much for ANr and not seen for ANc. As the number of diffraction orders increases, the diffraction signal will be greatly reduced. The appearance of the second-order diffraction peak indicates that the crystal quality of ANa is the best among three films, and ANr is better than ANc. This echoes the Raman result later.

3.2. Calculations of crystallite size, dislocation density and micro strain

The grain size (D) of AlN thin film can be calculated by the Scherrer's equation.

The (0002) half-width of the crystal plane is usually affected by screw dislocations, which characterizes the degree of inclination of each unit cell in the crystal with respect to the C-axis, and usually there is another kind of dislocation in the crystal, namely edge dislocations characterizing the degree of twist between the unit cells in the crystal. The dislocation density of AlN can be estimated by the following formula:

$$\delta = \frac{\beta^2_{(0002)}}{4.35b^2} \tag{1}$$

where b is the length of the Burgers vector ($b = 0.3110$ nm).

Furthermore, in order to study the micro strain between the films, the micro strain (ε) can be calculated by the following expression:

$$\varepsilon = \frac{\beta \cos\theta}{4} \tag{2}$$

with β: full-width at half-maximum (FWHM(2θ)).

Finally, we can get the grain size, dislocation density and microstrain of the AlN thin film grown on the A-plane sapphire as 22.41 nm, 2.0 nm^{-2} and 1.57%, respectively. The (0002) crystal plane usually characterizes the screw dislocation of the film. The dislocation density may be arisen due to the heteroepitaxy of AlN layer on foreign sapphire substrate with different lattice constants and thermal expansion coefficients. From our above measurements and calculations, it can be seen that the dislocation density and micro-strain of ANa are lower than those reported in the literature [2], indicating good crystalline perfection of our magnetron sputtering (MS)-deposited AlN films.

3.3. Optical properties of the deposited AlN films: bandgap and optical constant measurements

In order to study the thickness, band gap and optical constants of three AlN films, the VASE, a non-contact method, was used to determine the optical constants and thickness of the film by measuring the reflection on the surface or interface. The polarization state psi (ψ) and the increment Δ were applied to analyze the SE spectra [44]. In the wavelength range of 193–1600 nm, three AlN films were measured at varying angles between 50° and 70°. The constants describing optical properties include complex refractive index and complex permittivity, are defined as:

$$n^* = n + \mathrm{i}k \tag{3}$$

$$\varepsilon^* = \varepsilon_1 + \mathrm{i}\varepsilon_2 = \sin\theta^2 + \sin\theta^2 \tan\theta^2 \left(\frac{1-\rho}{1+\rho}\right)^2 = n^{*2} \tag{4}$$

where n is the refractive index, k is the extinction coefficient (imaginary part), ε_1 and ε_2 are the real and imaginary parts of the dielectric function, and θ is the angle of incidence, respectively [45].

SE spectra are fitted by using J A Woollam Co software to establish a physical model: roughness/AlN layer/AlN layer/sapphire substrate. The Brugman effective medium approximation is used to describe the surface roughness composed of 50% atmosphere and 50% AlN. The second AlN layer is composed of PSemi-MO Oscillator, PSemi-Tri Oscillator and Gaussian Oscillator, and the sapphire substrate adopts the sapphire ordinary model [46]. First, the Cauchy model was used to fit the transparent area to obtain its approximate thickness and roughness, and then the B-spline was used to fit the absorption part, step by step to the low wavelength direction, and finally the fitting result was vibrated. In the fitting process, the best fitting result is found by changing the thickness

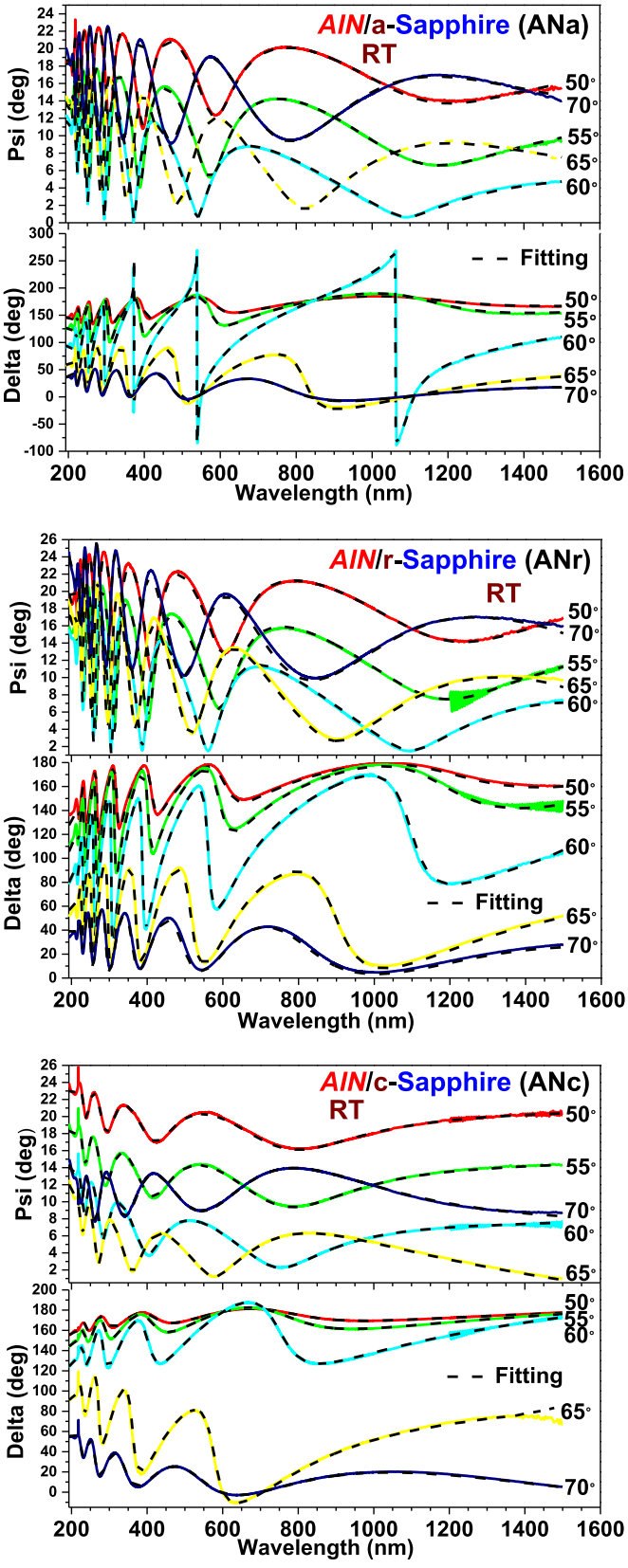

Figure 2. SE experimental data (color solid line) at RT and model fitting results (black dashed line) for three samples temperature.

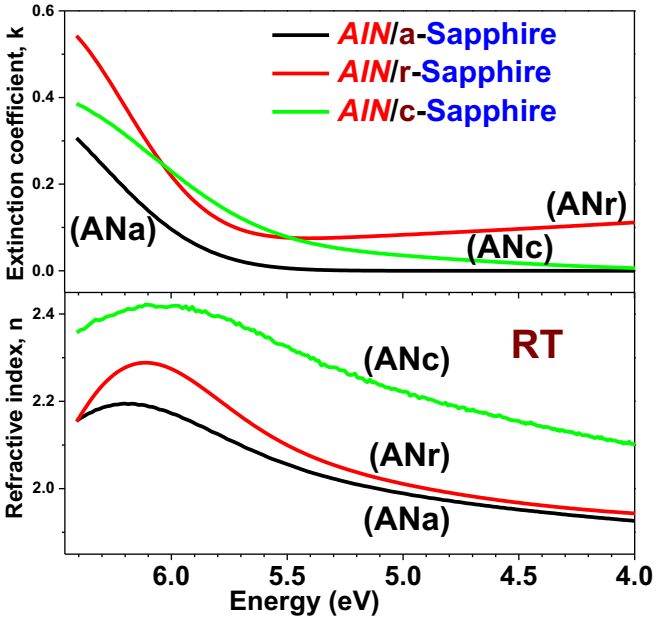

Figure 3. Fitted optical constants (n and k) of AlN at room temperature.

Table 1. The thickness, surface roughness and comparative bandgap values obtained from SE.

Sample	ANa	ANr	ANc
Band gap (eV)	6.17	6.08	6.03
Thickness (nm)	334.56	353.43	214.24
Roughness (nm)	11.53	19.39	4.90

and other parameters of all layers. The final minimum mean square error of ANa, ANr and ANc are 5.283, 12.840 and 3.245, respectively. As shown in figure 2, the fitting curves are in good agreement with the experimental spectra, and the fitting results are shown in the table 1.

It can be seen that the band gap of the three AlN films is basically around 6.0 eV, and the *a*-plane sapphire is slightly larger, which is basically close to the band gap of the AlN film reported in the literature [46]. Among the three films, the AlN film on the *C*-plane sapphire has the smallest roughness, and the AlN on the *R*-plane sapphire has the largest roughness. The reason for this phenomenon may be due to the incomplete integration of islands during the magnetron sputtering growth process. The refractive index and extinction coefficient of the three AlN films obtained by SE fitting change with wavelength are shown in figure 3. It can be seen that the refractive index of the three AlN films gradually decreases with the increase of wavelength, and the three films have the same dispersion relationship. From the fitting results, it can be found that the band gaps of ANa, ANr and ANc are 6.17 eV, 6.08 eV, and 6.03 eV, respectively; the thickness is 334.56 nm,

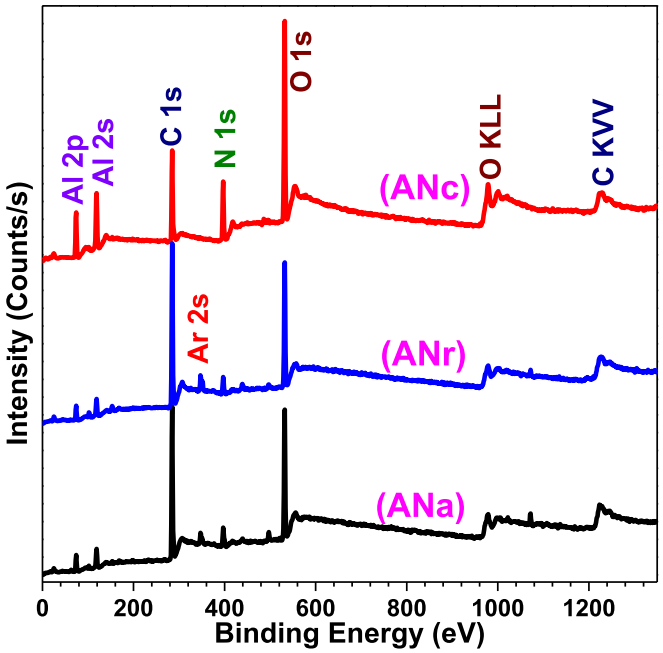

Figure 4. XPS survey spectra of AlN thin films ANa, ANr, and ANc.

353.43 nm, and 214.24 nm, respectively. This may be the result of the lattice mismatch inducing effect in the thinner film grown on the sapphire substrate. In other words, the thinner the AlN film, the worse the crystal order, the more defects, and the smaller the band gap. As reported in the literature, the thickness has an effect on the optical constants of the AlN film [47].

3.4. Chemical composition of the deposited AlN films: XPS spectra

Figure 4 shows the XPS spectra of three AlN films. It can be seen that these AlN films are composed of aluminum, nitrogen, carbon and oxygen. Secondly, you can also see a large amount of carbon and oxygen, which may be caused by air or impurities adsorbed on the sample surface [48]. Ar element may be caused by pollution during the preparation process.

The fitting analyses of the narrow spectra Al2p, N1s and O1s were carried out. Figure 5 shows the fitting spectra of the narrow N1s and O1s bands of three AlN films. By using XPSPEAK4.1 software [49], Gauss–Lorentz mixture was used. The function performing leads to a fitting analysis on them. The Shirley model [50–53] is selected as the background type. It can be seen that all spectra can be fitted to two sub-peaks of different chemical bonds. The fitting results of Al2p, N1s and O1s are shown in table 2.

For narrow-spectrum Al2p, it can be synthesized as two sub-peaks of Al–N bond and Al–O bond, respectively, for three AlN films with different polarities (ANa, ANr, ANc). The binding energies of Al–N are 74.390 eV, 74.180 eV and 74.199 eV; the binding energies of Al–O are 73.605 eV, 73.441 eV and 73.308 eV, respectively. For the narrow-band N1s, the two sub-peaks of different chemical states can also

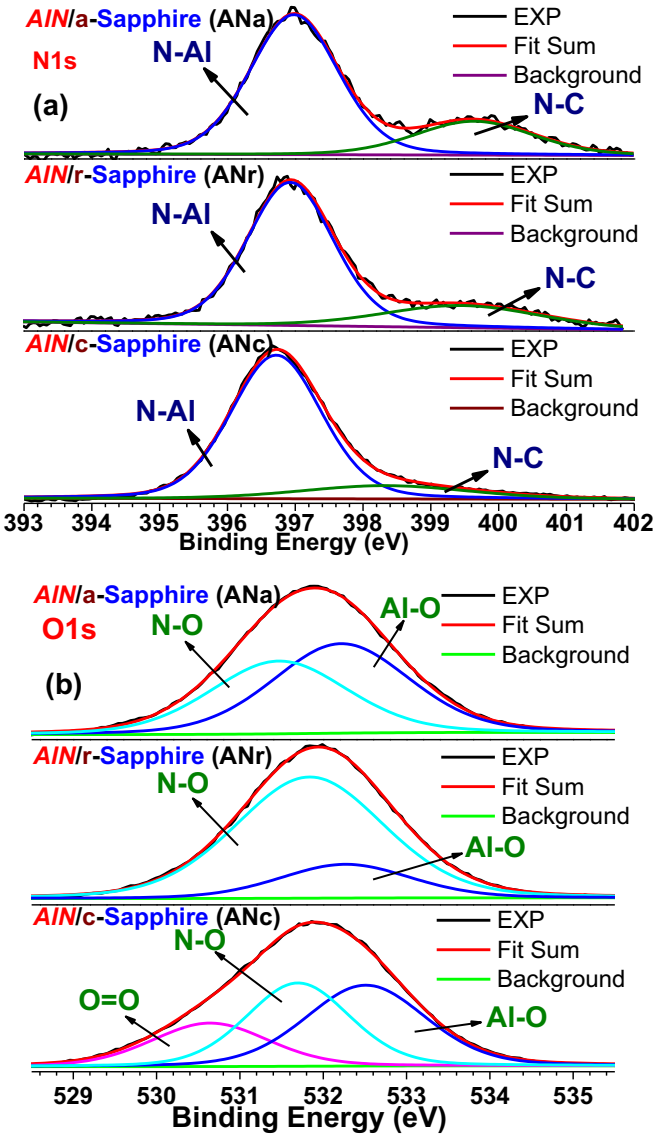

Figure 5. XPS fine scans on the peaks of (a) N1s and (b) O1s for three AlN thin films, ANc, ANr, and ANc, respectively.

be fitted by the same principle. The binding energies of N–Al are 396.982 eV, 396.934 eV and 396.720 eV; the binding energies of N–C are 399.638 eV, 399.466 eV and 398.334 eV, respectively for three films. For the narrow-band O1s, ANa and ANr are intended to synthesize two sub-peaks of different chemical states, while ANc is intended to synthesize three sub-peaks of different chemical states. The binding energies of N–O are 531.468 eV, 531.837 eV and 531.697 eV; the binding energies of Al–O are, respectively, 532.216 eV, 532.265 eV and 532.510 eV; the binding energy of O–O is 530.642 eV, respectively. These values are consistent with the reported results [54, 55]. From the fitting results, it can be found that the oxidized layer on the top of ANr is the least compared to that on ANa and ANc. Furthermore, it can be seen that the binding energy required for forming the same chemical bond between the three AlN films is different. Factors such as charge transfer effects, the presence of electric fields, hybridization and

Table 2. XPS analysis result for the AlN thin films.

Sample			ANa	ANr	ANc
Al2p	#1(Al–N)	B.E. (eV)	74.390	74.180	74.199
		Area	5196.842	6897.109	18 119.910
		FWHM	1.542	1.668	1.602
	#2(Al–O)	B.E. (eV)	73.605	73.441	73.308
		Area	6103.011	3392.278	15 189.160
		FWHM	1.432	1.254	1.343
N1s	#1(N–Al)	B.E. (eV)	396.982	396.934	396.720
		Area	12 363.950	12 192.650	39 694.040
		FWHM	1.532	1.495	1.580
	#2(N–C)	B.E. (eV)	399.638	399.466	398.334
		Area	3993.904	3437.839	6766.460
		FWHM	2.048	2.720	2.913
O1s	#1(Al–O)	B.E. (eV)	532.216	532.265	532.510
		Area	58 618.750	19 852.180	70 684.550
		FWHM	1.934	1.852	1.697
	#2(N–O)	B.E. (eV)	531.468	531.837	531.697
		Area	47 606.070	80 902.610	62 651.640
		FWHM	1.932	2.102	1.460
AlN_{Al}/AlN_N			1.190	0.409	1.129
d_{xps} (Å) (nm)			33.64	19.00	27.37

environmental charge density may all cause changes in binding energy. Among these factors, charge transfer is considered the main mechanism [48].

Through fitting analysis of all narrow spectra, the atomic ratio of these AlN films and the thickness of the surface oxide coating can be calculated. The Al:N ratio shows that AlN grown on the *A*-side sapphire has the highest Al content, while the AlN film grown on the *R*-side has the lowest Al content, as shown in table 2. The difference in the ratio may be attributed to the formation of a large amount of alumina on the AlN surface grown on the *A*-side sapphire, which can be verified by the correlation between the oxide thickness and Al/N. As oxygen is doped into the AlN film, the aluminum nitride film with a thicker surface oxide coating has a larger Al/N ratio.

Due to the high oxygen affinity of Al atoms, it is easy to form an oxide film on the surface [56], the thickness of the oxide film on the surface can be estimated by the following formula d (Å)

$$d_{xps}\,(\text{Å}) = \lambda_0 \sin\theta \ln\left(\frac{N_m I_0 \lambda_m}{N_0 I_m \lambda_0} + 1\right). \tag{5}$$

The ratio of the volume density of aluminum atoms to oxides in metal atoms is $N_m/N_0 = 1.6$ (calculated based on the densities of Al = 2.7 g cm^{-3} and Al_2O_3 = 3.1 g cm^{-3}), λ_0 and λ_m are alumina and the attenuation length of aluminum nitride [57], θ is 75°, and I_0/I_m is the ratio of the area of aluminum oxide to the area of aluminum nitride [2].

It can be seen that the thickness of the oxide film of ANr is the smallest, and the thickness of the oxide film of ANa is the largest. The different amount of surface oxygen contamination on AlN surface may be attributed to the different oxygen adsorption capacity. The oxygen content is consistent with the width of the E_2 (high) mode measured by Raman spectroscopy below [58].

3.5. Crystallinity of the deposited AlN films: Raman spectra (RS) and temperature-dependent Raman spectra (TD-RS) measurements

In order to characterize the defect density of three AlN films, RS spectroscopy is used to study and analyze it. In figure 6, two different wavelength lasers of 266 nm and 325 nm were used to excite the sample. The 266 nm light can basically only detect the top surface of the epitaxial AlN film, and the penetration depth of 325 nm light into AlN is much deeper than that of 266 nm light. It can be seen that there is a certain difference in the Raman spectra under two excitation wavelengths. For the AlN film (ANa) grown on the *A*-plane and *R*-plane sapphire, the Raman AlN E_2 (high) signal excited at 266 nm is stronger than the 325 nm excitation, but for the AlN film (ANc) grown on the *C*-plane sapphire, the E_2 (high) signal can be seen very weak. The orange-labeled peaks are derived from AlN thin films and are located near 650 cm^{-1}, and the rest are RS peaks of sapphire, which are consistent with those reported in the literature [59–61]. The E_2 (high) mode of the AlN film can be seen from the figure. The Raman characteristic peaks of the AlN film on a, *r*-plane sapphire are obviously stronger than those of the AlN film on the *c*-plane sapphire; for ANc, when using 266 nm and 325 nm excitation, only weak E_2 (high) signal can be detected.

Using Gaussian to fit the Raman spectrum excited at 266 nm, we can get the FWHM of the E_2 (high) mode of ANa, ANr and ANc at 11.92 cm^{-1}, 12.74 cm^{-1} and 12.88 cm^{-1}, respectively. The FWHM of Ana, ANr and ANc gradually increased, and the FWHM of AlN film on *C*-plane sapphire was the largest. The FWHM and intensity of the E_2 (high) peak

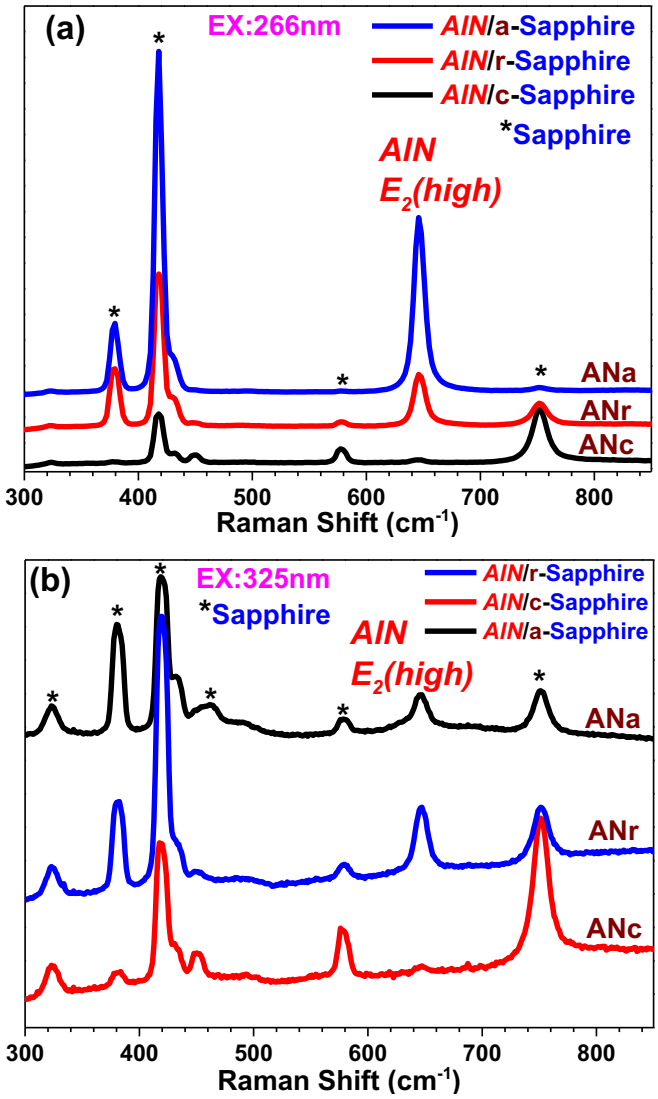

Figure 6. Raman spectra of AlN thin films on different surface orientation of sapphire. Use (a) 266 nm and (b) 325 nm two different wavelengths laser excitation.

of AlN are more sensitive to the crystal quality of AlN. With the increase of defects and dislocations, incident photons will be scattered randomly, resulting in a decrease in the intensity of the E_2 (high) peak and the peak width increases. Therefore, for three AlN films of different polarities grown by magnetron sputtering, the crystal quality of ANa is better than that of ANr and ANc, and the defect density is also less than that of ANr and ANc. Secondly, ANc can only detect a weak E_2 (high) peak, which may also be caused by an excessively thick surface oxide layer. It has been reported in the literature that in AlN films grown on *C, R*, and *A* sapphire substrates, the oxide layer on the surface of the AlN film grown on the *C*-plane sapphire substrate is the thickest, which is several times that of the *R* and *A* sapphire substrates under the same conditions [2]. This coincides with the previous XPS analysis results.

In addition, the E_2 (high) peak is not only sensitive to defects, but also extremely sensitive to changes in the stress of the film. We all know that for AlN films, the displacement of the E_2 (high) peak is usually used to characterize the stress of the film. The E_2 (high) peak of the AlN film is at 657.4 ± 0.2 cm^{-1}. It can be seen from figures 7(a)–(c) that E_2 (high) peaks are shifted to low wavenumber, that is to say, there are certain tensile stresses. The biaxial stress can be estimated by the following formula:

$$\sigma = \Delta\omega / K \tag{6}$$

where $\Delta\omega$ is the difference between the E_2 (high) phonon peak between the stressed and unstressed AlN epitaxial layer, and K (2.4 ± 0.2 cm^{-1} GPa^{-1}) is the strain coefficient [62, 63].

Figure 7 shows the variable temperature Raman (80–800 K) spectra measured on three AlN thin films using a 266 nm laser, with (a)–(c) for wide range (200–1000 cm^{-1}), while (a1)–(c1) for expanded range (620–680 cm^{-1}) on the AlN E_2 (high) phonon, respectively. The temperature interval was 30 K in each graph. The E_2 (high) mode can be clearly seen in all three films. It is obvious that as the temperature increases, the E_2 (high) mode moves to a low wave number, and the half-peak width gradually increases. It can be observed in the figure that when the temperature rises from 80 K to 300 K, the movement of the E_2 (high) mode is not obvious, and when the temperature exceeds 300 K, the E_2 (high) mode moves significantly. This shows that high temperature has a greater impact on AlN films. From low temperature to high temperature, the shifts of the RS peaks of ANa, ANr, and ANc are, respectively, indicating the temperature pair. Secondly, the main reason for the displacement of the scattering peak may be (a) as the temperature gradually increases, the non-harmonic vibration of phonons and the non-intermittent coupling between phonons will gradually increase; (b) the lattice thermal expansion effect. The above reasons will cause the change of the lattice vibration energy level, which will cause the corresponding shift of the RS peak frequency [64].

It is interesting to find some differences of the temperature (T) behaviors for three AlN films. Description and discussion at above paragraph are suitable for two samples ANc and ANr, i.e. for AlN films grown on *C*-plane and *R*-plane sapphire. However, for ANa, the AlN film grown on *A*-plane sapphire, a slight different T-variation of the Raman E_2 (high) mode can be revealed from figure 7(a1) that the Raman peak of ANa increases when heated from 80 to 350 K, and then reduces above 350 K.

By using Gaussian function to fit the Raman spectra of each temperature point, with the obtained results shown in figures 8(a)–(c), for three AlN films of ANa, ANr and ANc, respectively. For AlN films, the crystal quality and residual strain can be evaluated by line width and Raman shift. It can be seen that except for the Raman shift of the AlN film growing on the *A*-plane sapphire, it gradually shifts to a high wave number with the increase of temperature in the low temperature section, and the Raman shift of the two AlN films of ANr and ANc are all with the increase of temperature. Gradually move to a lower wave number, which is consistent with what is reported in the literature [64–66].

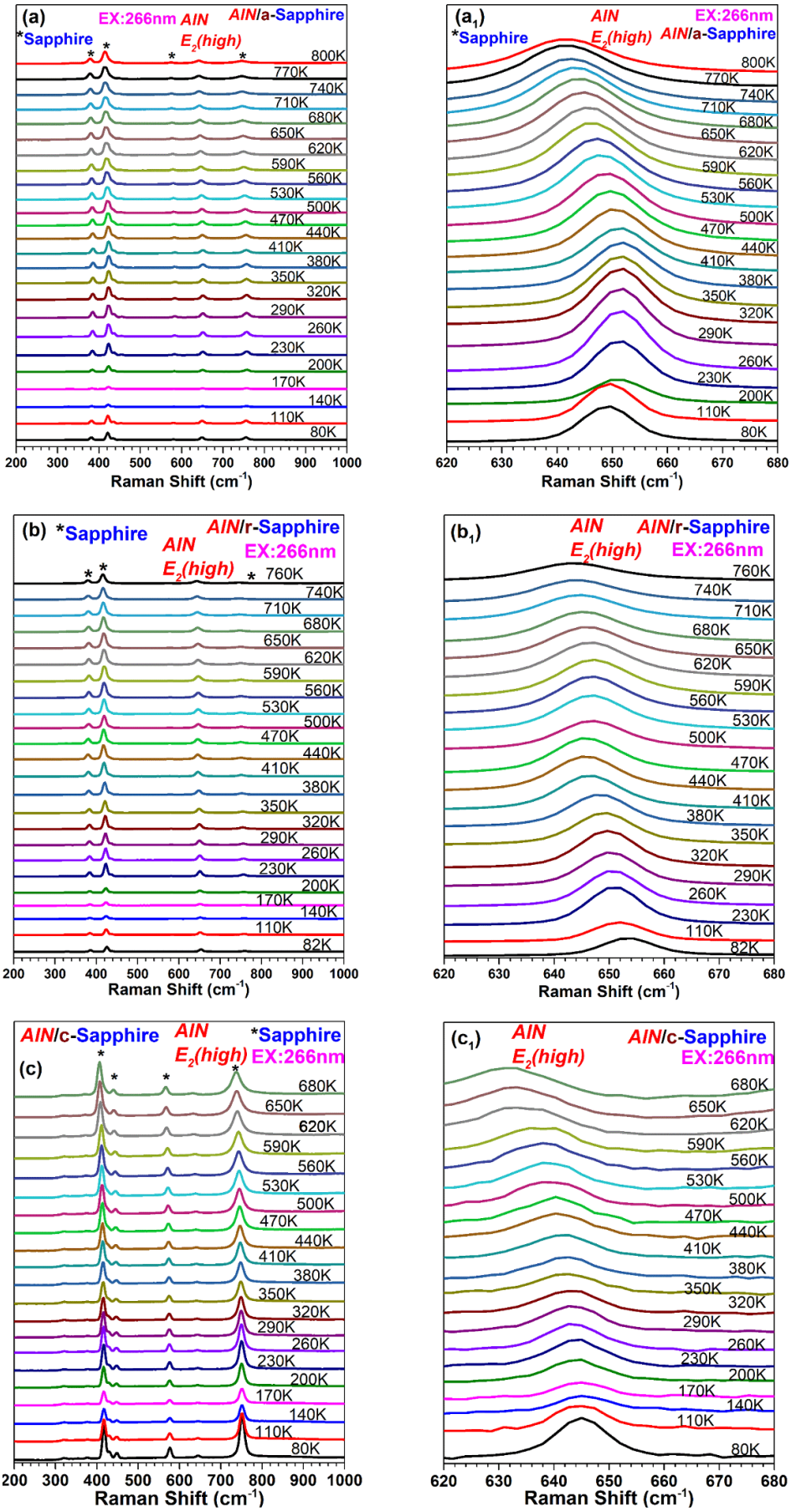

Figure 7. (a), (a_1), (b), (b_1), (c), (c_1) 266 nm laser excited temperature-dependent Raman spectra.

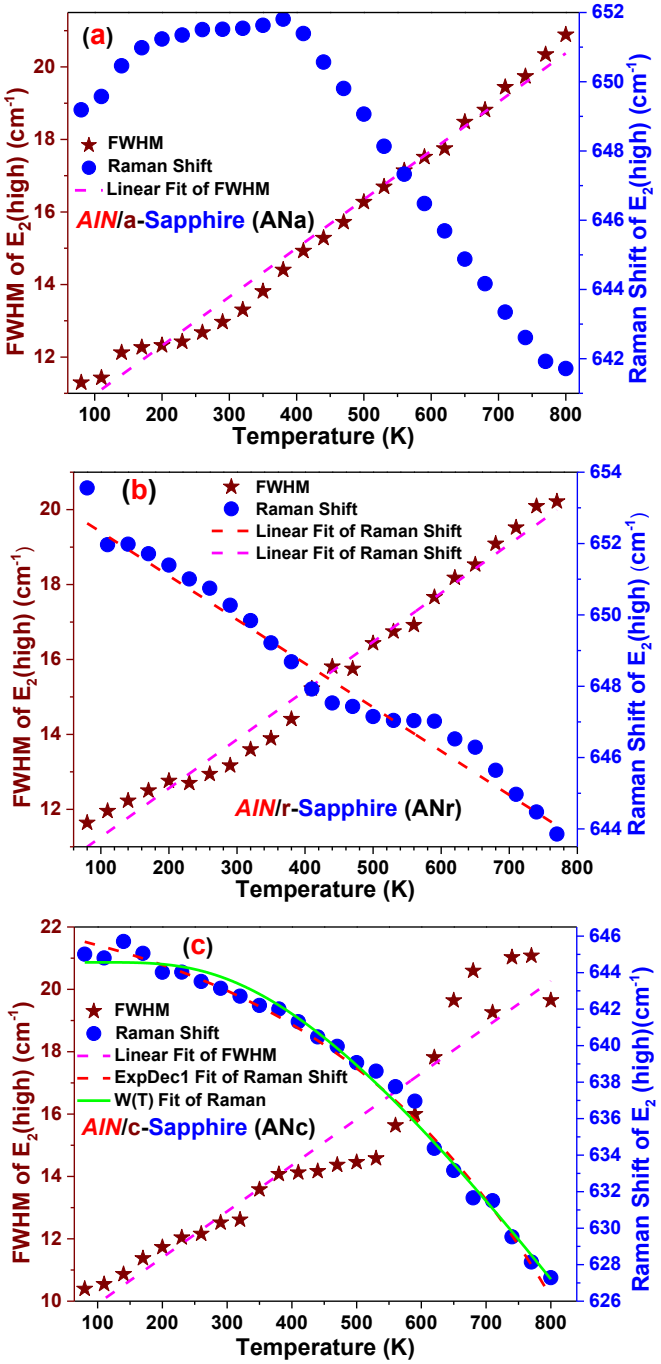

Figure 8. (a)–(c) Raman linewidth and shift of E_2 (high) as a function of temperature.

It is seen from figure 8(c), the T-variable curve of ANc for AlN/C-sapphire exhibits a similar T-dependence as for bulk AlN [66]. A T-dependent equation [66]:

$$\omega(T) = \omega_0 - A/\{\exp[B(hc\omega_0/k_BT) - 1]\} \qquad (7)$$

is adapted to fit the T-variable curve of ANc (AlN/C-sapphire) in figure 8(c). The fitted parameters are $\omega_0 = 644.56$ cm^{-1}, $A = 72.19$ cm^{-1} and $B = 1.42$. The fitted T-variable curve from equation (8) of ANc (AlN/C-sapphire) is displayed by solid (green) line in figure 8(c). For other

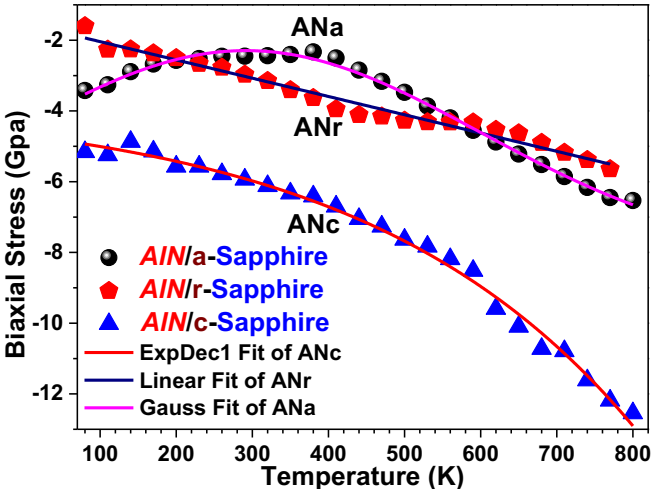

Figure 9. The dependences of stress in AlN films on temperature.

two cases of ANa and ANr, i.e. AlN/A-sapphire and AlN/R-sapphire, they are needed to explore new physical models.

The Raman phonon frequency decrease is attributed to the thermal expansion of the crystal lattice and the phonon–phonon interaction caused by the temperature increase. At the same time, the half-height width of the three AlN films gradually increases with the gradual increase in temperature, and the increase in Raman linewidth is basically related to the scattering of point defects [67]. Compared with ANa, ANr and ANc, the point defects of ANr are less than that of ANa and ANc. The gradual increase of the line width will also reduce the lifetime of the phonon, and the change of Raman displacement will also cause the change of the residual stress. The lifetime and strain of the phonon can be studied and analyzed further as followed.

Figure 9 is a graph showing the relationship between the stress of three AlN films and the temperature. The Raman spectra were measured with an excitation wavelength of 266 nm, and the above formula (6) was used to calculate the stress at each temperature point, and the relationship between the stress and the temperature can be obtained. From the figure, we can see that in the range of 80–800 K, three AlN films exhibit tensile stress. For ANa, it can be seen that its tensile stress will gradually decrease with the increase of temperature in the low temperature area, and its tensile stress will gradually increase with the increase of temperature in the high temperature area; look at ANr and ANc again, its tensile stress is in the entire range of 80–800 K, and it gradually increases with the increase of temperature. The difference is that the tensile stress of ANr is basically linear with temperature change trend, and the tensile stress of ANc presents a parabolic trend with increasing temperature. Secondly, the stress of the three AlN films changes most with temperature is the AlN film grown on the C-plane sapphire. The reason for these differences may be the mismatch of the sapphire substrate and the AlN epitaxial film, and the mismatch of the thermal expansion coefficients of the two. In general, the tensile stress of AlN films

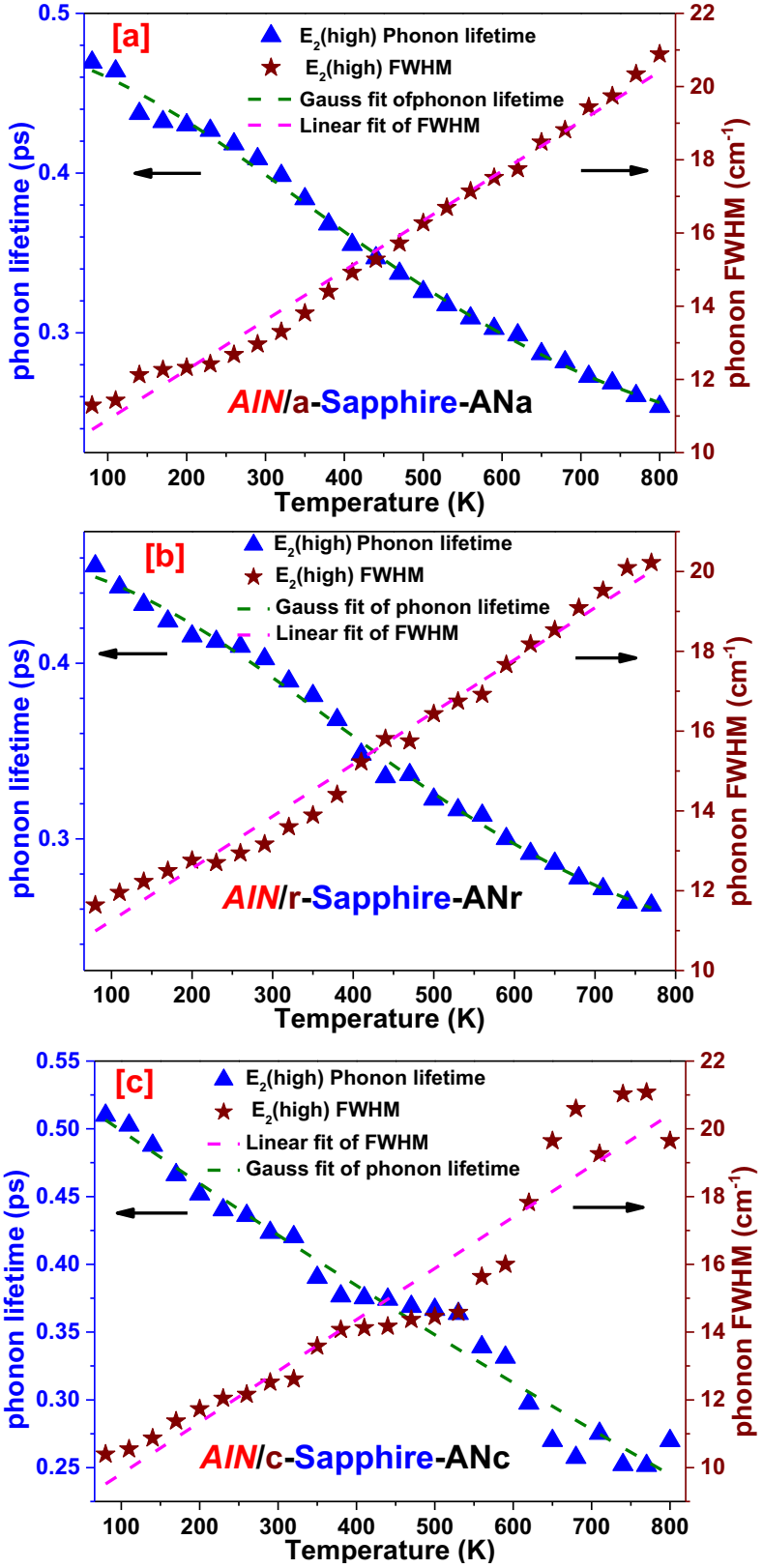

Figure 10. (a)–(c) Phonon lifetime and FWHM of the E_2 (high) phonon as function of temperature.

grown on *a*-plane and *r*-plane sapphire with temperature is smaller than that of AlN films grown on *c*-plane sapphire. This has important reference value for the research of AlN devices, although new and penetrative physics models are needed to explore further.

Finally, we can analyze its phonon lifetime through Raman, and understanding the dynamics of phonons is also particularly important for the devices designed by engineers. Phonons can determine the thermal phonon effect, and the thermal phonon effect has been shown to play a key role in carrier

relaxation. The phonon lifetime can be determined by the phonon linewidth and the energy time uncertainty relationship in the Raman experiment. The Lorentz function is used to fit the measured experimental spectrum to obtain the line width, and the following formula is used to estimate the phonon lifetime τ [68]:

$$\frac{\Delta E}{\hbar} = \frac{1}{\tau} \tag{8}$$

ΔE is the phonon line width, the unit is cm^{-1}, $\hbar = 5.3 \times 10^{-12}$ cm^{-1} s.

Figure 10 exhibits the relationship between the phonon lifetime of the E_2 (high) phonon and the temperature, for three AlN films of ANa, ANr and ANc, respectively. It can be seen from the figure that the lifetime of the phonon is inversely proportional to the half-width, and the lifetime of the E_2 (high) phonon decreases with increasing temperature. At 80 K, the measured E_2 (high) phonon lifetimes of ANa, ANr and ANc are 0.469 ps, 0.455 ps, and 0.509 ps, respectively. In a low temperature environment, the phonon lifetime is slightly longer than that in a high temperature environment. The basic mechanism affecting the lifetime of phonons is the anharmonic decay of one phonon to other Brillouin zone phonons, thus conserving energy and momentum. As we all know, phonon broadening is mainly caused by impurity phonon scattering and inharmonic attenuation. When the phonon lifetime decreases, the line width gradually increases. This is because the probability of phonon attenuation to low-energy phonon varies with temperature. As it rises, it increases, leading to the enhancement of the phonon anharmonic decay process. Compared with other two AlN films, in the same temperature range, the phonon lifetime of ANr varies with temperature less than that of ANa and ANc. Therefore, the phonon lifetime of ANr is less affected by temperature than ANa and ANc.

4. Conclusion

In summary, a series of AlN films were deposited on sapphire substrates with different crystal planes by magnetron sputtering. Various techniques, including XRD, SE, XPS and Raman, were used to characterize the optical, surface and material properties of these AlN films. XRD results showed that the main orientation of AlN is the (0002) plane, and the diffraction peak of the AlN film grown on the *A*-plane sapphire is stronger than that of the other two films, i.e. its crystal quality is better than the other two films. Also, the grain size, dislocation density and microstrain of ANa are obtained. The results obtained by room temperature SE show that the three AlN films have the same dispersion relationship. The band gap of the AlN film on the *A*-plane sapphire is the largest, and the band gap of the AlN film on the *C*-plane sapphire is the smallest; the roughness of the AlN film on the *C*-plane sapphire is the smallest, and the roughness of AlN on the *R*-face sapphire is the largest; the thickness of the AlN film on the *C*-face sapphire is smaller than other two. The defects of the AlN film grown on the *C* surface are higher than the other two films. The XPS analysis results tell us that the AlN film grown on the *A* side sapphire has the largest Al/N ratio, and the *R* side is the smallest. This shows that the thickness of the surface oxide film of ANa is the largest, and the Al atom on the surface has the largest oxygen affinity. From the results of room temperature Raman characterization, the RS peak of the AlN film on the *C*-plane sapphire is obviously weaker than that on the *A*-plane and *R*-plane sapphire. Comparison within three AlN films, the crystallinity of the AlN film grown on the *C*-plane sapphire is low, and its crystal quality is the worst; the AlN film grown on the *A*-plane sapphire has the best crystal quality. Finally, through the use of variable temperature Raman measurements, the Raman shifts of the three AlN films all move to a low wave number, and the half-value width gradually increases, with the increase of temperature. In the range of 80–800 K, all three AlN films exhibit tensile stress. It is just that the stress of ANc has the greatest influence with temperature, and their E_2 (high) phonon life is gradually declining. Our results and analyses, even quantitatively and in phenomenology, will provide a base for further penetrative research.

Acknowledgments

This work was supported by the National Natural Science Foundation of China (No. 51868002), and the project supported by State Key Laboratory of Luminescence and Applications (No. SKLA-2019-06).

ORCID iDs

Wei Guo https://orcid.org/0000-0002-6233-0529
Lingyu Wan https://orcid.org/0000-0002-9718-5595
Zhe Chuan Feng https://orcid.org/0000-0002-8982-8757

References

[1] Panda P, Ramaseshan R, Ravi N, Mangamma G, Jose F, Dash S, Suzuki K and Suematsu H 2017 Reduction of residual stress in AN thin films synthesized by magnetron sputtering technique *Mater. Chem. Phys.* **200** 78–84
[2] Li Y, Zhang C, Luo X, Liang Y, Wuu D-S, Tin C-C, Lu X, He K, Wan L and Feng Z C 2018 Surface, structural and optical properties of AlN thin films grown on different face sapphire substrates by metalorganic chemical vapor deposition *Appl. Surf. Sci.* **458** 972–7
[3] Yoshida H and Kimura S 2020 High-crystalline-quality AlN grown on SiC substrates by controlling growth mode *J. Cryst. Growth* **537** 125605
[4] Li F, Wang L, Yao W, Meng Y, Yang S and Wang Z 2020 Analysis of growth rate and crystal quality of AlN epilayers by flow-modulated metal organic chemical vapor deposition *Superlattices Microstruct.* **137** 106336
[5] Kuang X-P, Zhang H-Y, Wang G-G, Cui L, Zhu C, Jin L, Sun R and Han J-C 2012 AlN films prepared on 6H–SiC substrates under various sputtering pressures by RF reactive magnetron sputtering *Appl. Surf. Sci.* **263** 62–68
[6] Nomoto J, Tsuchiya T and Yamamoto T 2019 Well-defined (0001)-oriented aluminum nitride polycrystalline films on amorphous glass substrates deposited by ion plating with direct-current arc discharge *Appl. Surf. Sci.* **478** 998–1003

[7] Zheng W, Lin R, Ran J, Zhang Z, Ji X and Huang F 2018 Vacuum-ultraviolet photovoltaic detector *ACS Nano* **12** 425–31

[8] Zhu Y, Lin R, Zheng W, Ran J and Huang F 2020 Near vacuum-ultraviolet aperiodic oscillation emission of AlN films *Sci. Bull.* **65** 827–31

[9] Cong R, Wang J, Wang X, Zhang Y, Lu W, Zhao W, Wang Q, Liu X and Yu W 2020 Ferromagnetic anisotropy in scandium-doped AlN hierarchical nanostructures *J. Mater. Sci.* **55** 8325–36

[10] Liu L, Liu B, Edgar J H, Rajasingam S and Kuball M 2002 Raman characterization and stress analysis of AlN grown on SiC by sublimation *J. Appl. Phys.* **92** 5183–8

[11] Jin L, Wu H L, Zhang Y, Qin Z Y, Shi Y Z, Cheng H J, Zheng R S and Chen W H 2020 The growth mode and Raman scattering characterization of m-AlN crystals grown by PVT method *J. Alloys Compd.* **824** 153935

[12] Hu Y Y, Zhou T F, Zheng S N, Liu X H, Zhao J J, Su X J, Huang J, Qiu Y X, Zhang J C and Xu K 2016 Quasi-transverse optical phonon mode in self-generated semipolar AlN grains embedded in c-oriented AlN matrix grown on sapphire using hydride vapor phase epitaxy *J. Appl. Phys.* **119** 205707

[13] Gablech I, Svatos V, Caha O, Dubroka A, Pekarek J, Klempa J, Neuzil P, Schneider M and Sikola T 2019 Preparation of high-quality stress-free (001) aluminum nitride thin film using a dual Kaufman ion-beam source setup *Thin Solid Films* **670** 105–12

[14] Yang H, Zhang X, Wang S, Zhu M, Cui Y and Dai N 2014 Surface properties of AlN and Al_x Ga_{1-x} N epitaxial layers characterized by angle resolved x-ray photoelectron spectroscopy *J. Mater. Sci., Mater. Electron.* **26** 950–4

[15] Setter N *et al* 2006 Ferroelectric thin films: review of materials, properties, and applications *J. Appl. Phys.* **100** 051606

[16] Dong W, Ji X, Wang W, Li T, Huang J, Zhou T, Fan Y and Xu K 2019 Investigation of surface acoustic waves anisotropy on high-quality AlN/sapphire grown by hydride vapor phase epitaxy *Mater. Res. Express* **6** 095903

[17] Taniyasu Y, Kasu M and Makimoto T 2004 Field emission properties of heavily Si-doped AlN in triode-type display structure *Appl. Phys. Lett.* **84** 2115–7

[18] Jiang K, Sun X, Ben J, Shi Z, Jia Y, Chen Y, Zhang S, Wu T, Lü W and Li D 2020 Suppressing the luminescence of V-related point-defect in AlGaN grown by MOCVD on HVPE-AlN *Appl. Surf. Sci.* **520** 146369

[19] Oto T, Banal R G, Kataoka K, Funato M and Kawakami Y 2010 100 mW deep-ultraviolet emission from aluminium-nitride-based quantum wells pumped by an electron beam *Nat. Photon.* **4** 767–71

[20] Jeong H, Salas-Montiel R, Lerondel G and Jeong M S 2017 Indium gallium nitride-based ultraviolet, blue, and green lightemitting diodes functionalized with shallow periodic hole patterns *Sci. Rep.* **7** 45726

[21] Qi Y *et al* 2018 Fast growth of strain-free AlN on graphene-buffered sapphire *J. Am. Chem. Soc.* **140** 11935–41

[22] Xiao S, Suzuki R, Miyake H, Harada S and Ujihara T 2018 Improvement mechanism of sputtered AlN films by high-temperature annealing *J. Cryst. Growth* **502** 41–44

[23] Tanaka S, Shojiki K, Uesugi K, Hayashi Y and Miyake H 2019 Quantitative evaluation of strain relaxation in annealed sputter-deposited AlN film *J. Cryst. Growth* **512** 16–19

[24] Hirayama H 2005 Quaternary InAlGaN-based high-efficiency ultraviolet light-emitting diodes *J. Appl. Phys.* **97** 091101

[25] Paskova T, Birch J, Tungasmita S, Beccard R, Heuken M, Svedberg E B, Runesson P, Goldys E M and Monemar B 1999 Thick hydride vapour phase epitaxial GaN layers grown on sapphire with different buffers *Phys. Status Solidi a* **176** 415–9

[26] Edwards N V, Bremser M D, Davis R F, Batchelor A D, Yoo S D, Karan C F and Aspnes D E 1998 Trends in residual stress for GaN/AlN/6H–SiC heterostructures *Appl. Phys. Lett.* **73** 2808–10

[27] Liu B D, Bando Y, Wu A M, Jiang X, Dierre B, Sekiguchi T, Tang C C, Mitome M and Golberg D 2010 352 nm ultraviolet emission from high-quality crystalline AlN whiskers *Nanotechnology* **21** 7

[28] Zollner C J, Almogbel A, Yao Y, SaifAddin B K, Wu F, Iza M, DenBaars S P, Speck J S and Nakamura S 2019 Reduced dislocation density and residual tension in AlN grown on SiC by metalorganic chemical vapor deposition *Appl. Phys. Lett.* **115** 161101

[29] Zheng W, Zheng R S, Wu H L and Di Li F 2014 Strongly anisotropic behavior of A(1)(TO) phonon mode in bulk AlN *J. Alloys Compd.* **584** 374–6

[30] Zhao J, Hu H P, Lei Y, Wan H, Gong L Y and Zhou S J 2019 Heteroepitaxial growth of high-quality and crack-free AlN film on sapphire substrate with nanometer-scale-thick AlN nucleation layer for AlGaN-based deep ultraviolet light-emitting diodes *Nanomaterials* **9** 1634

[31] Tang B, Hu H P, Wan H, Zhao J, Gong L Y, Lei Y, Zhao Q and Zhou S J 2020 Growth of high-quality AlN films on sapphire substrate by introducing voids through growth-mode modification *Appl. Surf. Sci.* **518** 146218

[32] Wang M X *et al* 2019 High-temperature annealing induced evolution of strain in AlN epitaxial films grown on sapphire substrates *Appl. Phys. Lett.* **114** 112105

[33] Wang C C, Chiu M C, Shiao M H and Shieu F S 2004 Characterization of AlN thin films prepared by unbalanced magnetron sputtering *J. Electrochem. Soc.* **151** F252–6

[34] Alrashdan M H S, Hamzah A A, Majlis B Y and Aziz M F 2014 Aluminum nitride thin film deposition using DC sputtering *2014 IEEE Int. Conf. on Semiconductor Electronics (ICSE2014)* (Piscataway, NJ: IEEE) pp 72–75

[35] Iriarte G F 2010 Influence of the magnetron on the growth of aluminum nitride thin films deposited by reactive sputtering *J. Vac. Sci. Technol.* A **28** 193–8

[36] Kumari N, Singh A K and Barhai P K 2014 Study of properties of AlN thin films deposited by reactive magnetron sputtering *Int. J. Thin Films Sci. Technol.* **3** 43–49

[37] Auger M A, Vazquez L, Jergel M, Sanchez O and Albella J M 2004 Structure and morphology evolution of ALN films grown by DC sputtering *Surf. Coat. Technol.* **180** 140–4

[38] Wang X N, Wang Z Y, Tian W M, Han Y B and Yao N 2020 Optical properties of AlN films deposited by energy-filtering magnetron sputtering technique *Appl. Phys. Express* **13** 025502

[39] Wang Y, Yang S, Chang H, Li W, Chen X, Hou R, Yan J, Yi X, Wang J and Wei T 2020 Flexible graphene-assisted van der Waals epitaxy growth of crack-free AlN epilayer on SiC by lattice engineering *Appl. Surf. Sci.* **520** 146358

[40] Susilo N *et al* 2020 Improved performance of UVC-LEDs by combination of high-temperature annealing and epitaxially laterally overgrown AlN/sapphire *Photonics Res.* **8** 385275

[41] Yao L R and Lu F H 2013 Low vacuum deposition of aluminum nitride thin films by sputtering *Int. J. Appl. Ceram. Technol.* **10** 51–59

[42] Lee J W, Cuomo J J, Moody B F, Cho Y S and Keusseyan R L 2004 *MRS Online Proc. Libr.* **783** 510

[43] Iriarte G F, Rodriguez J G and Calle F 2010 Synthesis of c-axis oriented AlN thin films on different substrates: a review *Mater. Res. Bull.* **45** 1039–45

[44] Kazazis S A, Papadomanolaki E, Androulidaki M, Tsagaraki K, Kostopoulos A, Aperathitis E and Iliopoulos E 2016 Effect of rapid thermal annealing on polycrystalline

InGaN thin films deposited on fused silica substrates *Thin Solid Films* **611** 46–51
[45] Yang H, Liu Y, Luo X, Li Y, Wuu D-S, He K and Feng Z C 2019 Effects of growth temperature and thickness on structure and optical properties of Ga_2O_3 films grown by pulsed laser deposition *Superlattices Microstruct.* **131** 21–29
[46] Liu Y, Ghafari E, Jiang X, Feng Y, Feng Z C, Ferguson I and Liu N 2017 Temperature-dependent optical properties of AlN thin films by spectroscopy ellipsometry *MRS Adv.* **2** 323–8
[47] Motamedi P and Cadien K 2015 Structural and optical characterization of low-temperature ALD crystalline AlN *J. Cryst. Growth* **421** 45–52
[48] Yang H, Qian Y, Zhang C, Wuu D-S, Talwar D N, Lin H-H, Lee J-F, Wan L, He K and Feng Z C 2019 Surface/structural characteristics and band alignments of thin Ga_2O_3 films grown on sapphire by pulse laser deposition *Appl. Surf. Sci.* **479** 1246–53
[49] Zhang C *et al* 2019 Surface and optical properties of indium-rich InGaN layers grown on sapphire by migration-enhanced plasma assisted metal organic chemical vapor deposition *Mater. Res. Express* **6** 016407
[50] Xiang Y, Zhou C and Wang W 2017 Characterization of spin-coated gallium oxide films and application as surface passivation layer on silicon *J. Alloys Compd.* **699** 1192–8
[51] Ramana C V, Rubio E J, Barraza C D, Miranda Gallardo A, McPeak S, Kotru S and Grant J T 2014 Chemical bonding, optical constants, and electrical resistivity of sputter-deposited gallium oxide thin films *J. Appl. Phys.* **115** 043508
[52] Ghose S, Rahman M S, Rojas-Ramirez J S, Caro M, Droopad R, Arias A and Nedev N 2016 Structural and optical properties of β-Ga_2O_3 thin films grown by plasma-assisted molecular beam epitaxy *J. Vac. Sci. Technol.* B **34** 02L109
[53] Donmez I, Ozgit-Akgun C and Biyikli N 2013 Low temperature deposition of Ga_2O_3 thin films using trimethylgallium and oxygen plasma *J. Vac. Sci. Technol.* A **31** 01A110
[54] Motamedi P and Cadien K 2014 XPS analysis of AlN thin films deposited by plasma enhanced atomic layer deposition *Appl. Surf. Sci.* **315** 104–9
[55] Kim Y, Kim M S, Yun H J, Ryu S Y and Choi B J 2018 Effect of growth temperature on AlN thin films fabricated by atomic layer deposition *Ceram. Int.* **44** 17447–52
[56] Vergara L, Clement M, Iborra E, Sanz-Hervas A, Garcia-Lopez J, Morilla Y, Sangrador J and Respaldiza M A 2004 Influence of oxygen and argon on the crystal quality and piezoelectric response of AlN sputtered thin films *Diam. Relat. Mater.* **13** 839–42
[57] Alexander M R, Thompson G E, Zhou X, Beamson G and Fairley N 2002 Quantification of oxide film thickness at the surface of aluminium using XPS *Surf. Interface Anal.* **34** 485–9
[58] Lughi V and Clarke D R 2006 Defect and stress characterization of AIN films by Raman spectroscopy *Appl. Phys. Lett.* **89** 241911
[59] Tan B *et al* 2018 AlN gradient interlayer design for the growth of high-quality AlN epitaxial film on sputtered AlN/sapphire substrate *CrystEngComm* **20** 6557–64
[60] Zheng W, Zheng R, Huang F, Wu H and Li F 2015 Raman tensor of AlN bulk single crystal *Photonics Res.* **3** 38–43
[61] Solonenko D, Schmidt C, Stoeckel C, Hiller K and Zahn D R T 2019 The limits of the post-growth optimization of AlN thin films grown on Si(111) via magnetron sputtering *Phys. Status Solidi* b **257** 1900400
[62] Rong X, Wang X, Chen G, Pan J, Wang P, Liu H, Xu F, Tan P and Shen B 2016 Residual stress in AlN films grown on sapphire substrates by molecular beam epitaxy *Superlattices Microstruct.* **93** 27–31
[63] Kamarudzaman A, Bin Abu Bakar A S, Azman A, Omar A-Z, Supangat A and Talik N A 2020 Positioning of periodic AlN/GaN multilayers: effect on crystalline quality of a-plane GaN *Mater. Sci. Semicond. Process.* **105** 104700
[64] Wu H L, Zhao W, He C G, Zhang K, He L F and Chen Z T 2019 Growth of high quality AlN/sapphire templates with high growth rate using a medium-temperature layer *Superlattices Microstruct.* **125** 343–7
[65] Liu H N, Cong X, Lin M L and Tan P H 2019 The intrinsic temperature-dependent Raman spectra of graphite in the temperature range from 4K to 1000K *Carbon* **152** 451–8
[66] Hayes J M, Kuball M, Shi Y and Edgar J H 2000 Temperature dependence of the phonons of bulk AlN *Japan J. Appl. Phys.* **39** L710–2
[67] Long H *et al* 2019 High quality 10.6 μm AlN grown on pyramidal patterned sapphire substrate by MOCVD *Appl. Phys. Lett.* **114** 451–8
[68] Kuball M, Hayes J M, Shi Y and Edgar J H 2000 Phonon lifetimes in bulk AlN and their temperature dependence *Appl. Phys. Lett.* **77** 1958–60